

A kappa Model for Mainland France

John Douglas, Pierre Gehl, Luis Fabian Bonilla, Céline Gélis

▶ **To cite this version:**

John Douglas, Pierre Gehl, Luis Fabian Bonilla, Céline Gélis. A kappa Model for Mainland France. Pure and Applied Geophysics, 2010, 167 (11), p. 1303-1315. 10.1007/s00024-010-0146-5 . hal-00556627

HAL Id: hal-00556627

https://brgm.hal.science/hal-00556627

Submitted on 19 Jan 2011

HAL is a multi-disciplinary open access archive for the deposit and dissemination of scientific research documents, whether they are published or not. The documents may come from teaching and research institutions in France or abroad, or from public or private research centers.

L'archive ouverte pluridisciplinaire **HAL**, est destinée au dépôt et à la diffusion de documents scientifiques de niveau recherche, publiés ou non, émanant des établissements d'enseignement et de recherche français ou étrangers, des laboratoires publics ou privés.

A κ model for mainland France

John Douglas[1]*, Pierre Gehl[1], Luis Fabian Bonilla[2] & Céline Gélis[2]

1. BRGM — RNSC/RIS, 3 avenue C. Guillemin, BP 36009, 45060 Orléans Cedex 2, France.

2. IRSN — DEI/SARG/BERSSIN, BP 17, 92262 Fontenay-aux-Roses, France.

September 28, 2009

Abstract

An important parameter for the characterization of strong ground motion at high-frequencies (> 1 Hz) is kappa, κ, which models a linear decay of the acceleration spectrum, $a(f)$, in log-linear space (i.e. $a(f) = A_0 \exp(-\pi\kappa f)$ for $f > f_E$ where f is frequency, f_E is a low frequency limit and A_0 controls the amplitude of the spectrum). κ is a key input parameter in the stochastic method for the simulation of strong ground motion, which is particularly useful for areas with insufficient strong-motion data to enable the derivation of robust empirical ground-motion prediction equations, such as mainland France. Numerous studies using strong-motion data from western North America (WNA) (an active tectonic region where surface rock is predominantly soft) and eastern North America (ENA) (a stable continental region where surface rock is predominantly very hard) have demonstrated that κ varies with region and surface geology, with WNA rock sites having a κ of about 0.04 s and ENA rock sites having a κ of about 0.006 s. Lower κs are one reason why high-frequency strong ground motions in stable regions are generally higher than in active regions for the same magnitude and distance. Few, if any, estimates of κs for French sites have been published. Therefore, the purpose of this study is to estimate κ using data recorded by the French national strong-motion network (RAP) for various sites in different regions of mainland France. For each record, a value of κ is estimated by following the procedure developed by Anderson and Hough [1984]: this method is based on the analysis of the S-wave spectrum, which has to be performed manually, thus leading to some uncertainties. For the three French regions where most records are available (the Pyrenees, the Alps and the Côtes-d'Azur), a regional κ model is developed using weighted regression on the local geology (soil or rock) and source-to-site distance. It is found that the studied regions have a mean κ between the values found for WNA and ENA. For example, for the Alps region a κ value of 0.0254 s is found for rock sites, an estimate reasonably consistent with previous studies.

*Currently on teaching leave at: Earthquake Engineering Research Centre, University of Iceland, Austurvegur 2A, 800 Selfoss, Iceland.

Keywords: strong-motion data, kappa, high-frequency decay, France, RAP, near-surface attenuation

1 Introduction

As is the case for many regions with limited observational ground-motion databases, seismic hazard assessment in France is complicated by large epistemic uncertainty concerning the expected ground motion in future earthquakes. Thanks to the establishment in the past couple of decades of a reasonably dense national strong-motion network in the most seismically-active parts of France (the Réseau Accélérometrique Permanent, RAP) many thousands of accelerometric records are now freely available [Péquegnat et al., 2008]. Nevertheless, due to the relatively low earthquake occurrence rates in mainland France there are very few records from earthquakes with moment magnitude, M_w, greater than 5.0. Due to recognized differences in magnitude- and distance-scaling of ground motions from small and large earthquakes [e.g. Bommer et al., 2007, Cotton et al., 2008, and references therein] it is currently not possible to develop robust, fully-empirical ground-motion prediction equations (GMPEs) reliable for higher magnitudes based on these data. Three alternative methods for the estimation of earthquake ground motions in France could be applied: 1) assume that ground motions in France are similar to those in areas for which robust GMPEs (either empirical or simulation-based) have been proposed (e.g. California, Japan or Italy) [e.g. Cotton et al., 2006]; 2) develop simulation-based GMPEs using input parameters derived from seismological analyses, as, for example, have been developed for eastern North America [e.g. Atkinson and Boore, 2006]; or 3) adjust GMPEs developed for other regions to be more applicable to France through, for example, the hybrid empirical-stochastic technique [e.g. Campbell, 2003, Douglas et al., 2006] or the referenced empirical approach [Atkinson, 2008]. Up until now method 1 has been used almost universally for France, probably due to the lack of sufficient strong-motion data from which to derive input parameters required for methods 2 and 3. Methods 2 and 3 generally require estimating various parameters characterizing the earthquake source (e.g. the stress drop parameter $\Delta\sigma$ and the source spectral shape), the travel path (e.g. geometrical decay and Q) and the local site (e.g. shear-wave velocity profile and near-surface attenuation). Numerous previous studies have estimated one or more of these parameters for France or regions of France [e.g. Campillo et al., 1993, Drouet et al., 2005, 2008]. However, we know of no published studies explicitly reporting estimates of κ as introduced by Anderson and Hough [1984]. The site contribution to κ is commonly believed to be related to the attenuation (e.g. Q or damping) in the top couple of kms, although there is some evidence for decay of high frequencies due to

source properties related to the size of a cohesive zone at the crack tip [e.g. Papageorgiou and Aki, 1983, Tsai and Chen, 2000]. The effect of κ is to act as a high-frequency ($> 1\,\mathrm{Hz}$) filter on ground motions and, therefore, it is a critical parameter for the accurate estimation of, for example, peak ground acceleration. Consequently, in this article we estimate κ using hundreds of accelerometric records from mainland France.

One motivation for this study was the finding of Douglas et al. [2009], who presented an approach to constrain the shear-wave velocity profile by making use of all available information on site conditions at a site of interest (e.g. soil type and depth to bedrock). They found that even when the shear-wave velocity profile is precisely known, the high-frequency site amplification is not. Douglas et al. [2009] attributed this, at first sight surprising, result to a lack of constraint on the near-surface attenuation. In their analysis they modelled attenuation by κ estimated using the empirical relationship of Silva et al. [1998] connecting κ and $V_{s,30}$ (the average shear-wave velocity of the top 30 m); this relationship had a large associated standard deviation that led to the large uncertainty in the high-frequency site amplification. If κ could be better estimated at a given site then there is the potential to significantly reduce this uncertainty. Therefore, in this article we investigate κ to see whether it can be better constrained for French sites.

This article starts with a section describing the strong-motion data used; next we describe our method for the evaluation of κ from the Fourier spectra of these data including an approach to estimate the accuracy of the estimated κs due to the subjectivity of the adopted methodology; following that we investigate the dependence of κ on source-to-site distance, region and local site conditions; and finally we conclude.

2 Data used

In order to concentrate on data of engineering interest and to limit the number of records analyzed, only records from earthquakes with magnitudes (any scale) larger than about 3.5 were downloaded from the RAP online strong-motion database (`http://www-rap.obs.ujf-grenoble.fr/`). Each acceleration time-history was then visually inspected and poor quality records (due to noise or severe baseline problems) on any of the three components were rejected from further consideration. In total 263 triaxial records (i.e. 789 components) from 30 earthquakes and 83 different stations were retained for analysis (Table 1 and Figure 1). Note that κs were computed for all three components. Earthquake locations given in the RAP database were used here since these are from local networks (mainly the French national RéNaSS catalogue) and, in addition, most available data are from considerable source-to-site distances and, therefore,

accurate hypocentral locations are not critical for this analysis.

Most of the records selected were recorded by stations in the three most seismically-active regions of France: the Pyrenees (110 records), the Alps (82 records) and the Côtes-d'Azur (51 records) (although sometimes the earthquake recorded occurred in a different region). Possible regional dependence of κ between these different areas is examined in Section 5. Other regions contribute few records and therefore they are not examined separately.

According to the classifications given on the RAP website, 178 of the selected records are from rock stations, 75 are from soil stations and 10 are from borehole stations. Note that, although κs were estimated from borehole records they were not used to derive the following models. Possible dependence of κ on the local site conditions is investigated in Section 5. A number of stations have recorded multiple earthquakes, which allows a station-specific κ model to be established. Specifically in Section 5 we develop such models for 11 stations that have recorded more than five earthquakes amongst those selected: OGAN (6 records), OGMO (8), OGMU (7), OGSI (6), PYAD (9), PYAT (9), PYFE (7), PYLO (9), PYLS (11), PYOR (8) and PYPR (8).

[Table 1 about here.]

[Figure 1 about here.]

3 Method used to estimate κ

In this study the classic method of estimating κ developed by Anderson and Hough [1984] is used. It is slightly modified due to the use of high-quality digital records from small events rather than analogue records from moderate and large earthquakes as used by Anderson and Hough [1984], like done by Hough et al. [1988], for a comparable dataset). Each component of a triaxial record is processed individually. The first step is to remove the mean and plot the acceleration time-history. Time-histories that are too noisy or have other problems are rejected. Next, the pre-event, P-wave and S-wave portions of the time-history are selected by eye. Then the Fourier amplitude acceleration spectra of each of these three portions are computed and plotted on the same graph with a logarithmic y-axis (amplitude) and a linear x-axis (frequency). Based on the S-wave spectra two frequencies are selected by visual inspection: f_E, the start of the linear downward trend in the acceleration S-wave spectrum, and f_X, the end of the linear downward trend or when the S-wave spectrum approaches the noise spectrum (i.e. when the signal-to-noise ratio becomes too small for the spectral amplitudes to be reliable). Figure 2 shows an example of a spectra with a clear high-frequency linear trend and low noise levels and the f_E and f_X frequencies chosen for this record by one of the analysts. We find

that f_E is generally around 3 Hz but with a large scatter (within the 2–12 Hz range used by Anderson and Hough [1984]). Thanks to the high resolution and low noise levels of the selected records f_X is generally in the range 20–50 Hz. The final step in the procedure is to fit, using standard least-squares regression, a line fitting the acceleration spectrum between f_E and f_X, from whose slope κ is given by $\kappa = -\lambda/\pi$ where λ is the slope of the best-fit line. Generally there is a sufficient frequency range between f_E and f_X to give a robust estimate of κ.

[Figure 2 about here.]

A non-automatic procedure for estimating κ was adopted because we noted that the frequency, f_E, at which the acceleration spectral amplitudes show a decline varied significantly from record to record and therefore assuming a constant f_E, such as been done in some previous studies, could lead to biased estimates for κ. Similarly, due to varying signal-to-noise ratios (visually inspected), f_X shows large variations and therefore it was not possible to use a constant value for all records. Since the procedure followed here is non-automatic it is quite time-consuming and also subjective because analysts can have different views on the selection of the pre-event, P-wave and S-wave portions of the record (although we found that differences in this stage did not significantly affect the κs obtained) and on the selection of f_E and f_X, which can lead to large variations in κ between analysts.

A semi-automatic procedure to choose the intervals used to compute the direct shear-wave spectra and noise spectra was also applied. Since both P- and S-wave arrival times had been previously picked, time windows of 5 s for the pre-event noise and direct S-wave were used to compute the Fourier spectra. Various lengths of time windows from 1 to 10 s were also tested with similar results, so a standard length of 5 s was finally chosen. The time series were processed using a Hanning taper of 5%. The resulting Fourier spectra were then smoothed by a Konno and Ohmachi [1998] filter (filter bandwidth of 40), and only data having a signal-to-noise ratio greater than three were used to compute κ. The values of f_X and f_E used to compute κ in this procedure were chosen by the analyst, as in the completely manual approach described above. In the next section we present the approach we took to quantify the subjectivity and precision of the obtained κs.

In the absence of the high-frequency decay quantified here by κ Fourier amplitude spectra should be flat above the corner frequency, f_c, of the source. When fitting the best-fit lines to determine κ it is necessary that f_E (the frequency chosen as the start of the best-fit line) is greater than f_c otherwise the κ estimates can be biased. When using strong-motion data from moderate and large earthquakes ($M_w \geq 5.5$) as done by Anderson and Hough [1984] f_c is generally lower than 1 Hz hence bias in κ due to f_c is not a problem. However, in this study

where we are using data from earthquakes with $3.4 \leq M \leq 5.3$ f_c is generally between 1 and 6 Hz, using Figure 8 of Drouet et al. [2008] showing the relation between magnitude and f_c. The f_E values selected here based on the observed spectra are greater than 2 Hz and, therefore, most of the best-fit lines will be unaffected by f_c, especially since f_X (the frequency up to which the line is fitted) is usually greater than 30 Hz.

Site amplification curves, relative to reference sites displaying little amplification, for some of the stations considered here are provided by Drouet et al. [2008]. Some of these curves show peaks in the site amplifications at high frequencies where they could complicate the estimation of κ (e.g. > 5 Hz), e.g. PYAD, PYBA and QUIF (see Figure 3). In our analysis we attempted to compensate for the peak in the Fourier amplitude spectra from such stations to avoid biasing the obtained κs (as done by Anderson and Hough [1984] for Santa Felicia Dam, with a similar high-frequency amplification). The relative site amplification curves for 49 stations provided by Drouet et al. [2008] could be used to correct the observed spectra as done by Margaris and Boore [1998], for example, but this has not been attempted for simplicity and in order to be consistent between all records, even those from stations not analyzed by Drouet et al. [2008]. Parolai and Bindi [2004] conduct simulations assuming a 1D single sedimentary layer overlaying a bedrock half-space and earthquakes with $2 \leq M_w \leq 6$ to examine the effect of local site amplification on κ estimates. They find that in the presence of strong site amplifications at frequencies greater than 4 Hz, it is necessary to fit the best-fit line to determine κ over a wide frequency band (e.g. 10–34 Hz) in order to obtain accurate κs. Thanks to the high resolution (24 bits) and low noise levels on the digital accelerograms used in this study we are generally able to extend the fitting of the best-fit lines to 30 Hz or higher. Therefore, it is likely that most κ estimates found here are not biased by high-frequency site effects. However, the combination of high-frequency site effects and higher noise levels at some RAP stations means that some κ values obtained in this study may be too high (see Section 5).

[Figure 3 about here.]

3.1 Variability in κ estimates

The first three authors of this article independently processed (the first two using the non-automatic procedure and the third the semi-automatic technique) the 263 records and their estimated κs were compared. It was found that for most records the estimated κs of the three analysts were similar (within $10 - 20\%$ of one another) but for some records with no clear linear amplitude dependence on frequency the measured κ vary greatly (up to 50%). After discussion some of these large differences were reduced by one or two analysts reprocessing the problem records. However, there remains a subjective aspect to the estimation of κ. Therefore,

due to the potentially large variability in κ estimates we do not believe that it is possible to make conclusions concerning κs for individual sites or earthquakes unless they are based on a large number of records. Therefore, in this study we only seek conclusions based on many records. Note that, as discussed above, if the best-fit lines are estimated over a frequency band affected by high-frequency site amplifications or high corner frequencies, κ estimates could be biased either upwards or downwards. In this situation, whatever method is used to average the estimates from each analyst the κs obtained will not be correct. As stated above we do not think that this is the situation for the vast majority of the records we analyzed.

By analyzing the three κ estimates from a single record it was found that the error in the measurement of an individual κ were multiplicative rather than additive, i.e. κ estimates from each analyst were higher or lower than the average κ by a certain percentage (e.g. 20%) rather than by an absolute amount (e.g. 0.005 s). Assuming multiplicative errors also has the benefit of excluding the possibility of predicting negative κs. Therefore, the logarithms of the six κ estimates for an individual record (from three analysts and for the two horizontal components) were computed and the mean and standard deviations computed from these six logarithms were used in the subsequent analysis. By averaging κs for both horizontal components we make the assumption that κ is the same for both components and hence it is independent of the azimuth of the incoming waves. The mean κs and associated standard deviations were then used to undertake weighted regression analysis using diagonal weighting matrices derived from the inverse variances of each κ estimate [e.g. Draper and Smith, 1998]. Since the variances are derived from the logarithms of the κs but the regression was performed on the untransformed κs (to be consistent with previous studies) the weighting matrices are slightly incorrect with respect to the regression performed, but we do not believe that this significantly affects the results. A traditional, non-weighted least squares regression was also computed in order to see the effect of the uncertainty measured on the κ values. To our surprise, both regressions are quite similar. The results of these regression analyses are reported below.

3.2 κ estimates from vertical components

κ was computed for the three components of ground motion but only the horizontal components were used to develop the κ models. Figure 4 shows the relation between the κ values computed using the horizontal and vertical components. The error bar for each measurement has also been plotted. This figure shows that vertical estimates are slightly smaller than the horizontal ones but, in general, the estimates are similar. Smaller κs from vertical components could be due to higher corner frequencies in vertical spectra compared to those from horizontal components. In absence of three-component stations, κ values obtained from vertical components may be

helpful for a first estimate of this parameter.

[Figure 4 about here.]

4 Distance dependence

The first-order model that is often fitted to κ estimates is: $\kappa = \kappa_0 + m_\kappa r_{\rm epi}$, where $r_{\rm epi}$ is epicentral distance and κ_0 and m_κ are constants [e.g. Anderson and Hough, 1984]. κ_0 is believed to be station-dependent and related to the near-surface attenuation in the top couple of km under the site whereas m_κ is believed to be region-dependent and related to the regional attenuation. As mentioned above in this study we have used the estimated standard deviations of each κ value to apply weighted regression analysis to find κ_0 and m_κ for our data. The results from non-weighted regression are also shown in the legend of the corresponding figures for completeness.

As a first step regression analysis is performed for all surface records (263 records) using the form: $\kappa = \kappa_{0,\rm rock} S_{\rm rock} + \kappa_{0,\rm soil} S_{\rm soil} + m_\kappa r_{\rm epi}$, where $S_{\rm rock} = 1$ for rock stations and 0 otherwise and $S_{\rm soil} = 1$ for soil stations and 0 otherwise. By using this functional form we allow near-surface attenuation at rock stations to be different from that at soil stations but we assume that the regional attenuation is the same since a common m_κ is used for rock and soil sites. The estimated κs with respect to $r_{\rm epi}$ and site class are shown in Figure 5 along with the fitted lines. The equations of the best-fit lines are:

$$\begin{aligned} \kappa_{\rm soil} &= 0.0270 + 0.000175\, r_{\rm epi} \\ \kappa_{\rm rock} &= 0.0207 + 0.000175\, r_{\rm epi}. \end{aligned} \quad (1)$$

Note that if these models are used in SMSIM [Boore, 2005], for example, then it is not also necessary to apply Q attenuation since this is already included in these κ models. However, it is standard practice when using SMSIM to use only the κ_0 terms and model the regional attenuation through a Q model.

Hough et al. [1988] present equations for estimating a two-layer Q model from κ_0 and m_κ values. Their approach has not been applied here because the values found using this method assume that Q is independent of frequency, which has not previously been found in France [e.g. Campillo et al., 1985, Drouet et al., 2008]. The Q tomography technique of Hough and Anderson [1988] has not been attempted since the distribution of data with respect to distance is insufficient and, in addition, there is not enough resampling of travel paths.

[Figure 5 about here.]

5 Regional dependence

There are sufficient records from the Pyrenees (109 records), the Alps (88 records) and the Côte d'Azur (50 records) to derive individual best-fit equations for these regions. Figure 6 shows the κ values for these three regions for both soil and rock conditions. The regional m_κ values are relatively close to each other. However, one clearly sees that the Pyrenees presents a lower attenuation than the Alps and both are less attenuated than the Côte d'Azur. These results are in agreement with regional attenuation studies in France using the isoseismal distribution from historical earthquakes [e.g. Baumont and Scotti, 2006] and previous Q estimates by Drouet et al. [2008], who find lower Q values for the Alps (322), i.e. faster attenuation, than for the Pyrenees (376).

[Figure 6 about here.]

These differences between regions are also observed on the κ_0 values for stations located on rock but the stations in the Alps show a larger attenuation than the other two regions for stations located on soil. This may be explained by the fact that some of the stations are located in the sedimentary Grenoble basin where the deep soil layer could lead to large attenuation.

Figures 7 and 8 show κ estimates and fitted linear relations for 11 stations located in the Alps and the Pyrenees. Two sets of fits were made: one in which the slope (κ_0) and the intercept (m_κ) were unconstrained and one in which m_κ was fixed to the value obtained from the regional analysis reported in Figure 6 and a corresponding κ_0 found. Considering the unconstrained fits, for stations located in the Alps, all of which are located on rock, m_κ shows variations up to a factor of two but they are relatively close to the m_κ estimated for this region (Figure 6) whereas conversely, for stations located in the Pyrenees (Figure 8) the variability of m_κ is larger. Concerning κ_0 the values for stations in the Alps (Figure 7) present similar values to those obtained for the whole region (Figure 6). An interesting exception is station OGMU whose κ_0 value for the unconstrained fits is quite close to the soil estimate in this region. This could be due to a site effect at about 10 Hz for this station [Drouet et al., 2008], which could bias upwards the estimates of κ [Parolai and Bindi, 2004]. Stations located in the Pyrenees present a larger variation of κ_0 with respect to the value computed for the whole region. This variability may come from structural differences beneath each station or perhaps from statistical variations in small sample sizes. Given the variation in the distribution of records with respect to distance between stations, the fits in which m_κ is constrained to its regional value are probably more reliable. These fits suggest that κ_0 for some Pyreneean rock stations (e.g. PYAT, PYLS and PYOR) is lower than at the average rock station.

[Figure 7 about here.]

[Figure 8 about here.]

6 Conclusions

In this article we have estimated the high-frequency attenuation parameter κ [Anderson and Hough, 1984] from 263 high-quality triaxial accelerograms from the French RAP strong-motion network. Furthermore we have investigated the dependence of κ on distance, region and site conditions to develop simple κ models for use in seismic hazard assessment for mainland France. We have found that the three studied regions (the Pyrenees, the Alps and the Côtes-d'Azur) present different yet relatively close similar dependency of κ on epicentral distance. The influence of local geology is slight yet noticeable.

The values obtained here are reasonably consistent with, although larger than (meaning higher attenuation), the 0.015 s and 0.0125 s values obtained for Switzerland by Bay et al. [2003] and Bay et al. [2005] , respectively, and the 0.012 s value for the western Alps found by Morasca et al. [2006], using a different technique. This could be attributed to more competent rock (higher shear-wave velocities) in Switzerland than in France. In contrast our average κ_0 is lower than the 0.05 s value found by Malagnini et al. [2000] for central Europe (mainly Germany).

Based on these results, in terms of near-surface attenuation it seems that mainland France lies between WNA (where κ has been found to be around 0.04 for rock sites) and ENA (where κ has been found to be much lower, 0.006 is a commonly used value). Similarly Campillo et al. [1985] concluded that their Q model situates France between ENA and WNA in terms of regional attenuation. This seems reasonable with respect to the seismotectonics of France (mainly a stable continental region but with areas of active tectonics, the Pyrenees and the Alps) and its geology (quite hard bedrock sites). Therefore, seismic hazard assessments for France could be conducted using a suite of GMPEs including some models from active tectonic regions (such as western North America) and some from stable continental regions (such as eastern North America) with their associated κ modified (downwards for models from active regimes and upwards for models from stable continental regions).

7 Acknowledgements

This study was funded by BRGM research and public service projects and a grant from the Réseau Accélérometrique Permanent (RAP) of France. The strong-motion networks in France are operated by various organizations (see RAP website), under the aegis of the RAP. The RAP data centre is based at Laboratoire de Géophysique Interne et de Tectonophysique, Grenoble.

We are very grateful to the personnel of these organizations for operating the stations and providing us with the data, without which this study would have been impossible. Finally, we thank Stéphane Drouet, Glenn Biasi and David Boore for careful and detailed reviews of an earlier version of this article and Stéphane Drouet for his GMT script to draw maps of epicentral and station locations and travel paths.

References

J. G. Anderson and S. E. Hough. A model for the shape of the Fourier amplitude spectrum of acceleration at high frequencies. *Bulletin of the Seismological Society of America*, 74(5): 1969–1993, Oct 1984.

G. M. Atkinson. Ground-motion prediction equations for eastern North America from a referenced empirical approach: Implications for epistemic uncertainty. *Bulletin of the Seismological Society of America*, 98(3):1304–1318, Jun 2008. doi: 10.1785/0120070199.

G. M. Atkinson and D. M. Boore. Earthquake ground-motion prediction equations for eastern North America. *Bulletin of the Seismological Society of America*, 96(6):2181–2205, 2006. doi: 10.1785/0120050245.

D. Baumont and O. Scotti. On the impact of the binning strategy on macroseismic magnitude-depth-I_0 estimates. In *Proceedings of First European Conference on Earthquake Engineering and Seismology (a joint event of the 13th ECEE & 30th General Assembly of the ESC)*, Sep 2006. Abstract CS2-625.

F. Bay, D. Fäh, L. Malagnini, and D. Giardini. Spectral shear-wave ground-motion scaling in Switzerland. *Bulletin of the Seismological Society of America*, 93(1):414–429, 2003.

F. Bay, S. Wiemer, D. Fäh, and D. Giardini. Predictive ground motion scaling in Switzerland: Best estimates and uncertainties. *Journal of Seismology*, 9:223–240, 2005.

J. J. Bommer, P. J. Stafford, J. E. Alarcón, and S. Akkar. The influence of magnitude range on empirical ground-motion prediction. *Bulletin of the Seismological Society of America*, 97 (6):2152–2170, 2007. doi: 10.1785/0120070081.

D. M. Boore. SMSIM — Fortran programs for simulating ground motions from earthquakes: Version 2.3 — A revision of OFR 96-80-A. Open-File Report 00-509, United States Geological Survey, Aug 2005. Modified version, describing the program as of 15 August 2005 (Version 2.30).

K. W. Campbell. Prediction of strong ground motion using the hybrid empirical method and its use in the development of ground-motion (attenuation) relations in eastern North America. *Bulletin of the Seismological Society of America*, 93(3):1012–1033, 2003.

M. Campillo, J.-L. Plantet, and M. Bouchon. Frequency-dependent attenuation in the crust beneath central France from *Lg* waves: Data analysis and numerical modeling. *Bulletin of the Seismological Society of America*, 75(5):1395–1411, Oct 1985.

M. Campillo, B. Feignier, M. Bouchon, and N. Béthoux. Attenuation of crustal waves across the Alpine Range. *Journal of Geophysical Research*, 98(B2):1987–1996, Feb 1993.

F. Cotton, F. Scherbaum, J. J. Bommer, and H. Bungum. Criteria for selecting and adjusting ground-motion models for specific target regions: Application to central Europe and rock sites. *Journal of Seismology*, 10(2):137–156, Apr 2006. doi: 10.1007/s10950-005-9006-7.

F. Cotton, G. Pousse, F. Bonilla, and F. Scherbaum. On the discrepancy of recent European ground-motion observations and predictions from empirical models: Analysis of KiK-net accelerometric data and point-sources stochastic simulations. *Bulletin of the Seismological Society of America*, 98(5):2244–2261, Oct 2008. doi: 10.1785/0120060084.

J. Douglas, H. Bungum, and F. Scherbaum. Ground-motion prediction equations for southern Spain and southern Norway obtained using the composite model perspective. *Journal of Earthquake Engineering*, 10(1):33–72, 2006.

J. Douglas, P. Gehl, L. B. Bonilla, O. Scotti, J. Régnier, A.-M. Duval, and E. Bertrand. Making the most of available site information for empirical ground-motion prediction. *Bulletin of the Seismological Society of America*, 99(3):1502–1520, Jun 2009. doi: 10.1785/0120080075.

N. R. Draper and H. Smith. *Applied Regression Analysis*. John Wiley & Sons, 3rd edition, 1998.

S. Drouet, A. Souriau, and F. Cotton. Attenuation, seismic moments, and site effects for weak-motion events: Application to the Pyrenees. *Bulletin of the Seismological Society of America*, 95(5):1731–1748, Oct 2005. doi: 10.1785/0120040105.

S. Drouet, S. Chevrot, F. Cotton, and A. Souriau. Simultaneous inversion of source spectra, attenuation parameters, and site responses: Application to the data of the French Accelerometric Network. *Bulletin of the Seismological Society of America*, 98(1):198–219, Feb 2008. doi: 10.1785/0120060215.

S. E. Hough and J. G. Anderson. High-frequency spectra observed at Anza, California: Implications for Q structure. *Bulletin of the Seismological Society of America*, 78(2):692–707, Apr 1988.

S. E. Hough, J. G. Anderson, J. Brune, F. Vernon III, J. Berger, J. Fletcher, L. Haar, T. Hanks, and L. Baker. Attenuation near Anza, California. *Bulletin of the Seismological Society of America*, 78(2):672–691, Apr 1988.

K. Konno and T. Ohmachi. Ground-motion characteristics estimated from spectral ratio between horizontal and vertical components of microtremor. *Bulletin of the Seismological Society of America*, 88(1):228–241, Feb 1998.

L. Malagnini, R. B. Herrmann, and K. Koch. Regional ground-motion scaling in central Europe. *Bulletin of the Seismological Society of America*, 90(4):1052–1061, Aug 2000.

B. N. Margaris and D. M. Boore. Determination of $\Delta\sigma$ and κ_0 from response spectra of large earthquakes in Greece. *Bulletin of the Seismological Society of America*, 88(1):170–182, Feb 1998.

P. Morasca, L. Malagnini, A. Akinci, D. Spallarossa, and R. B. Herrmann. Ground-motion scaling in the western Alps. *Journal of Seismology*, 10(3):315–333, 2006. doi: 10.1007/s10950-006-9019-x.

A. S. Papageorgiou and K. Aki. A specific barrier model for the quantitative description of inhomogeneous faulting and the prediction of strong ground motion. Part I. Description of the model. *Bulletin of the Seismological Society of America*, 73(3):693–702, Jun 1983.

S. Parolai and D. Bindi. Influence of soil-layer properties on κ evaluation. *Bulletin of the Seismological Society of America*, 94(1):349–356, Feb 2004.

C. Péquegnat, P. Guéguen, D. Hatzfeld, and M. Langlais. The French Accelerometric Network (RAP) and National Data Centre (RAP-NDC). *Seismological Research Letters*, 79(1):79–89, Jan/Feb 2008.

W. Silva, R. Darragh, N. Gregor, G. Martin, N. Abrahamson, and C. Kircher. Reassessment of site coefficients and near-fault factors for building code provisions. Technical Report Program Element II: 98-HQ-GR-1010, Pacific Engineering and Analysis, El Cerrito, USA, 1998.

C.-C. P. Tsai and K.-C. Chen. A model for the high-cut process of strong-motion accelerations in terms of distance, magnitude, and site condition: An example from the SMART 1 array, Lotung, Taiwan. *Bulletin of the Seismological Society of America*, 90(6):1535–1542, Dec 2000.

List of Figures

1 Epicentral (circles) and station (triangles) locations and travel paths (lines) of the records used for this study. 16

2 Example of direct shear-wave and noise spectra computed from a record that shows a clear high-frequency linear trend. Also shown are the intervals used to estimate the pre-event noise and the direct shear-wave spectra (black parts of acceleration time-history) and the frequencies f_E and f_X chosen by one of the analysts (the other analysts chose similar f_E and f_X for records such as this). . 17

3 Example of direct shear-wave and noise spectra computed from a record used in the analysis that shows a high-frequency site effect (and hence it is difficult to estimate a reliable κ from this record). Also shown are the intervals used to estimate the pre-event noise and the direct shear-wave spectra (black parts of acceleration time-history) and the frequencies f_E and f_X chosen by one of the analysts (f_E and f_X for records such as this varied between analysts). 18

4 Comparison of κ values computed from vertical and horizontal components. ± 1 standard deviation bars are also plotted. The dashed line represents the 1:1 relation. 19

5 Distance dependence of κ for all stations for soil and rock conditions. The vertical lines represent the standard deviation of six independent measurements of κ (three estimates, two horizontal components). Results for κ_0 and m_κ from standard (solid line) and weighted (dashed line) least squares regressions are shown in the legend of each plot. 20

6 Distance dependence of κ values for three regions in mainland France. The top plots present the results for stations located on soil. The bottom plots show the results for stations located on rock. 21

7 κ estimates and their ± 1 standard deviations for stations located in the Alps. Also shown are the fitted linear relations. Four best-fit lines were fitted for each station: two (using standard and weighted regression) in which m_κ was allowed to vary (black) and two (using standard and weighted regression) in which m_κ was constrained to the value from the regional analysis shown in Figure 6 (grey). 22

8 κ estimates and their ± 1 standard deviations for stations located in the Pyrenees. Also shown are the fitted linear relations. Four best-fit lines were fitted for each station: two (using standard and weighted regression) in which m_κ was allowed to vary (black) and two (using standard and weighted regression) in which m_κ was constrained to the value from the regional analysis shown in Figure 6 (grey). 23

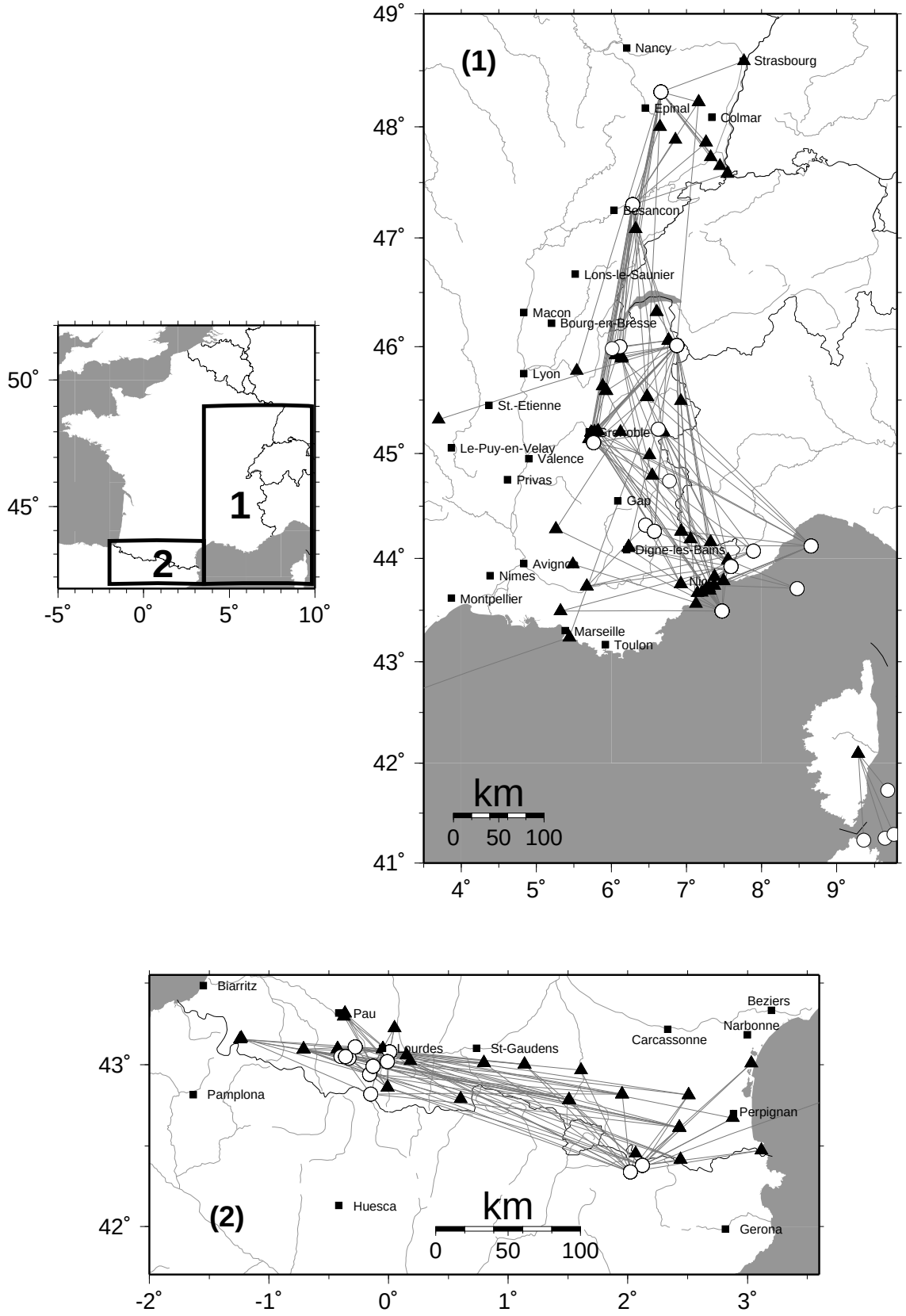


Figure 1: Epicentral (circles) and station (triangles) locations and travel paths (lines) of the records used for this study.

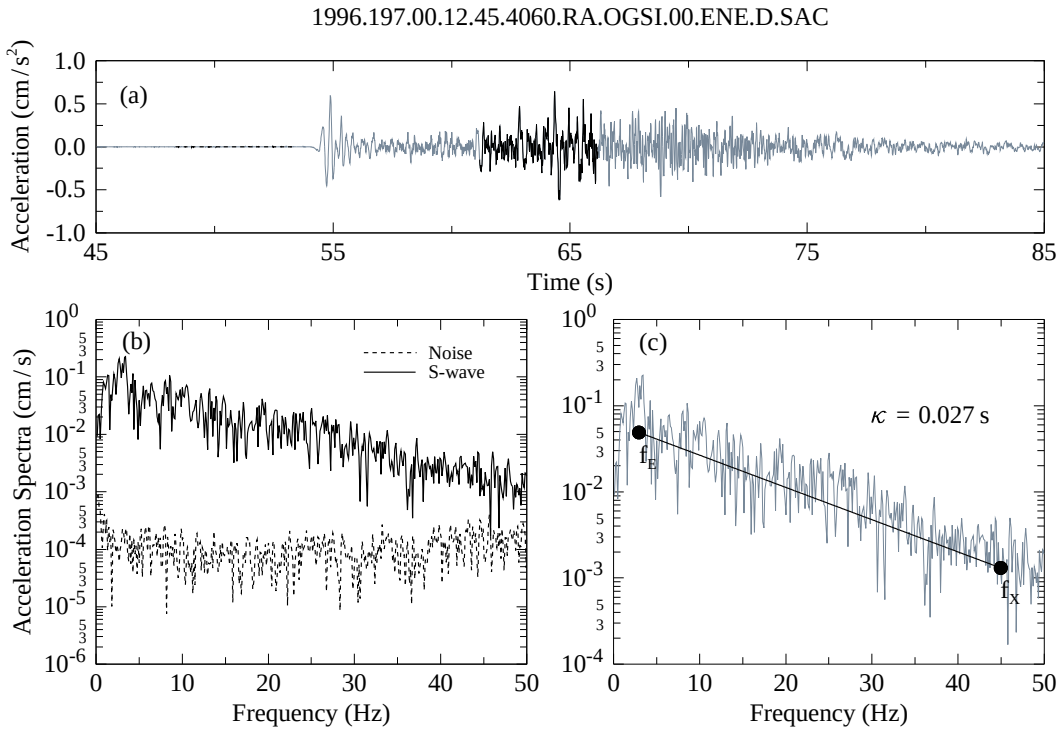


Figure 2: Example of direct shear-wave and noise spectra computed from a record that shows a clear high-frequency linear trend. Also shown are the intervals used to estimate the pre-event noise and the direct shear-wave spectra (black parts of acceleration time-history) and the frequencies f_E and f_X chosen by one of the analysts (the other analysts chose similar f_E and f_X for records such as this).

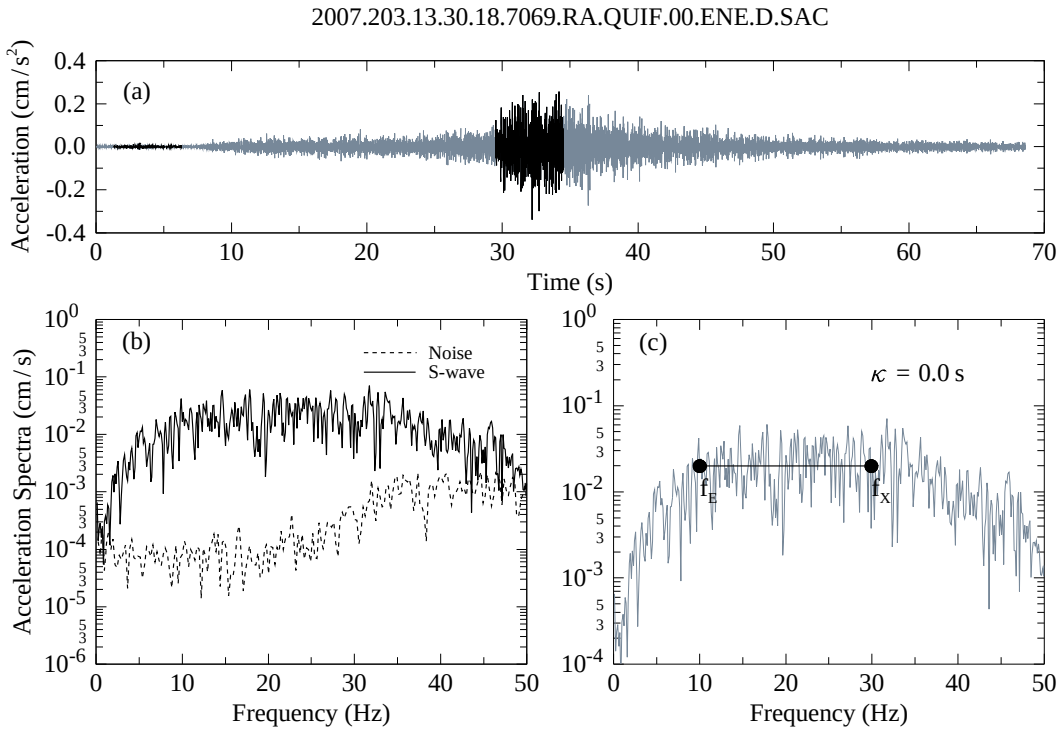


Figure 3: Example of direct shear-wave and noise spectra computed from a record used in the analysis that shows a high-frequency site effect (and hence it is difficult to estimate a reliable κ from this record). Also shown are the intervals used to estimate the pre-event noise and the direct shear-wave spectra (black parts of acceleration time-history) and the frequencies f_E and f_X chosen by one of the analysts (f_E and f_X for records such as this varied between analysts).

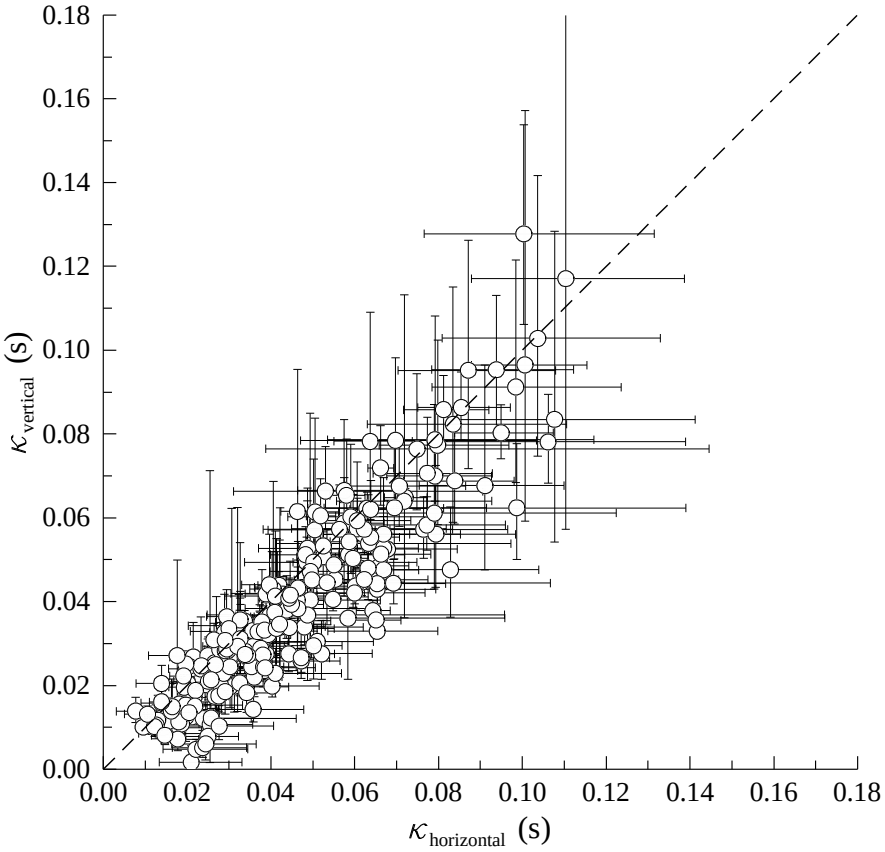


Figure 4: Comparison of κ values computed from vertical and horizontal components. ± 1 standard deviation bars are also plotted. The dashed line represents the 1:1 relation.

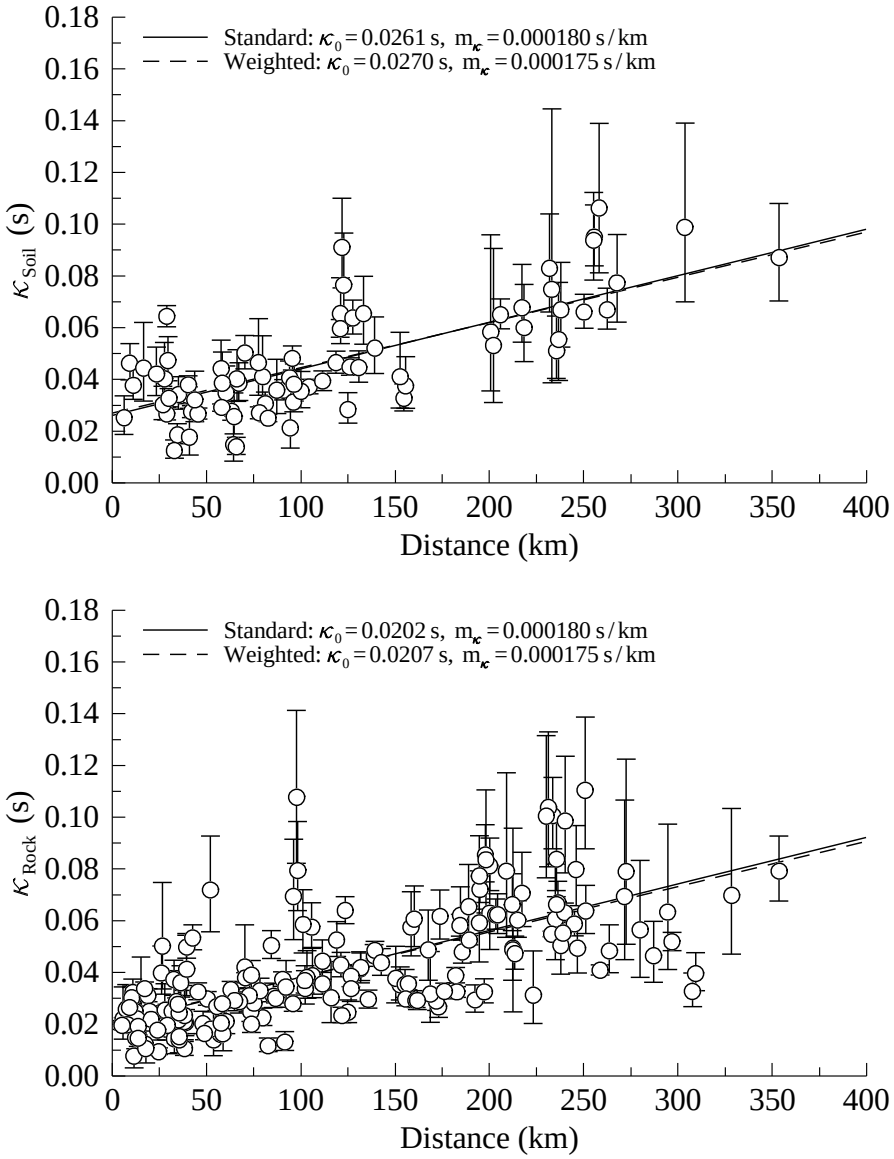


Figure 5: Distance dependence of κ for all stations for soil and rock conditions. The vertical lines represent the standard deviation of six independent measurements of κ (three estimates, two horizontal components). Results for κ_0 and m_κ from standard (solid line) and weighted (dashed line) least squares regressions are shown in the legend of each plot.

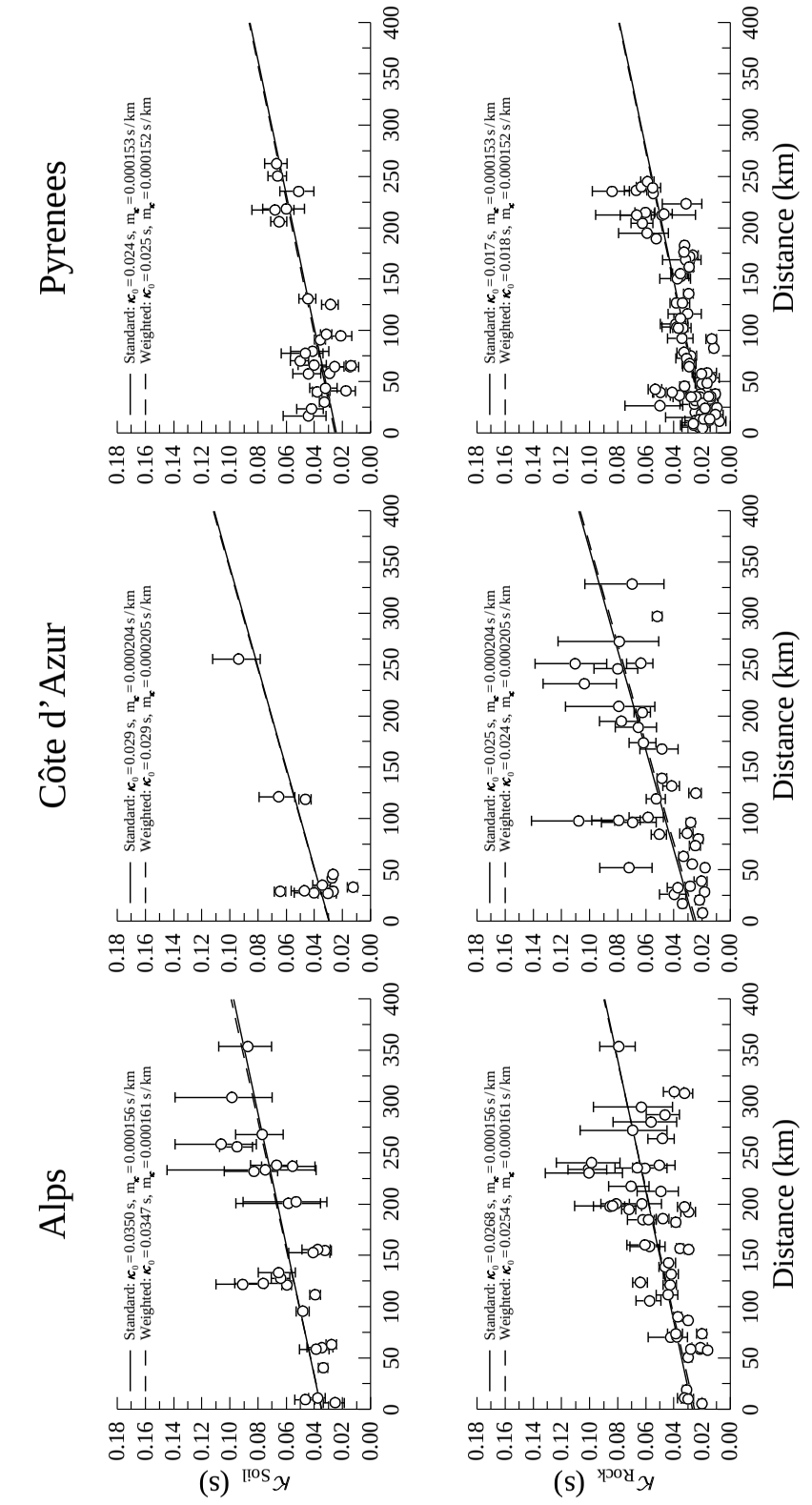


Figure 6: Distance dependence of κ values for three regions in mainland France. The top plots present the results for stations located on soil. The bottom plots show the results for stations located on rock.

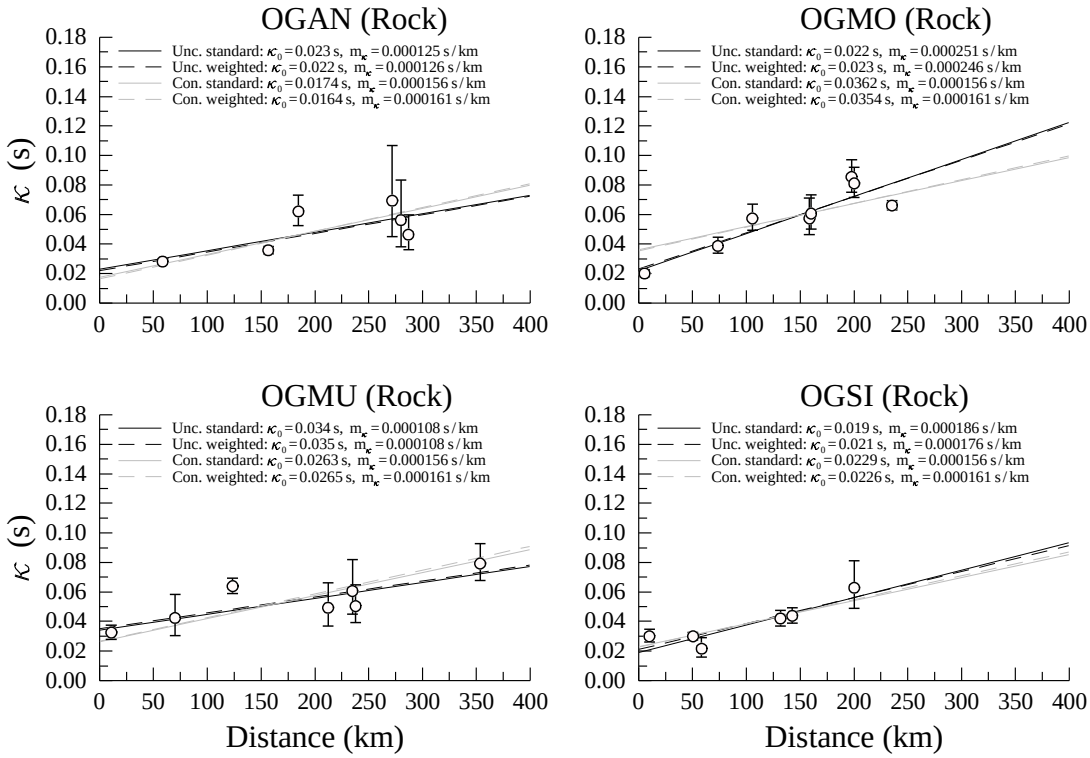


Figure 7: κ estimates and their ± 1 standard deviations for stations located in the Alps. Also shown are the fitted linear relations. Four best-fit lines were fitted for each station: two (using standard and weighted regression) in which m_κ was allowed to vary (black) and two (using standard and weighted regression) in which m_κ was constrained to the value from the regional analysis shown in Figure 6 (grey).

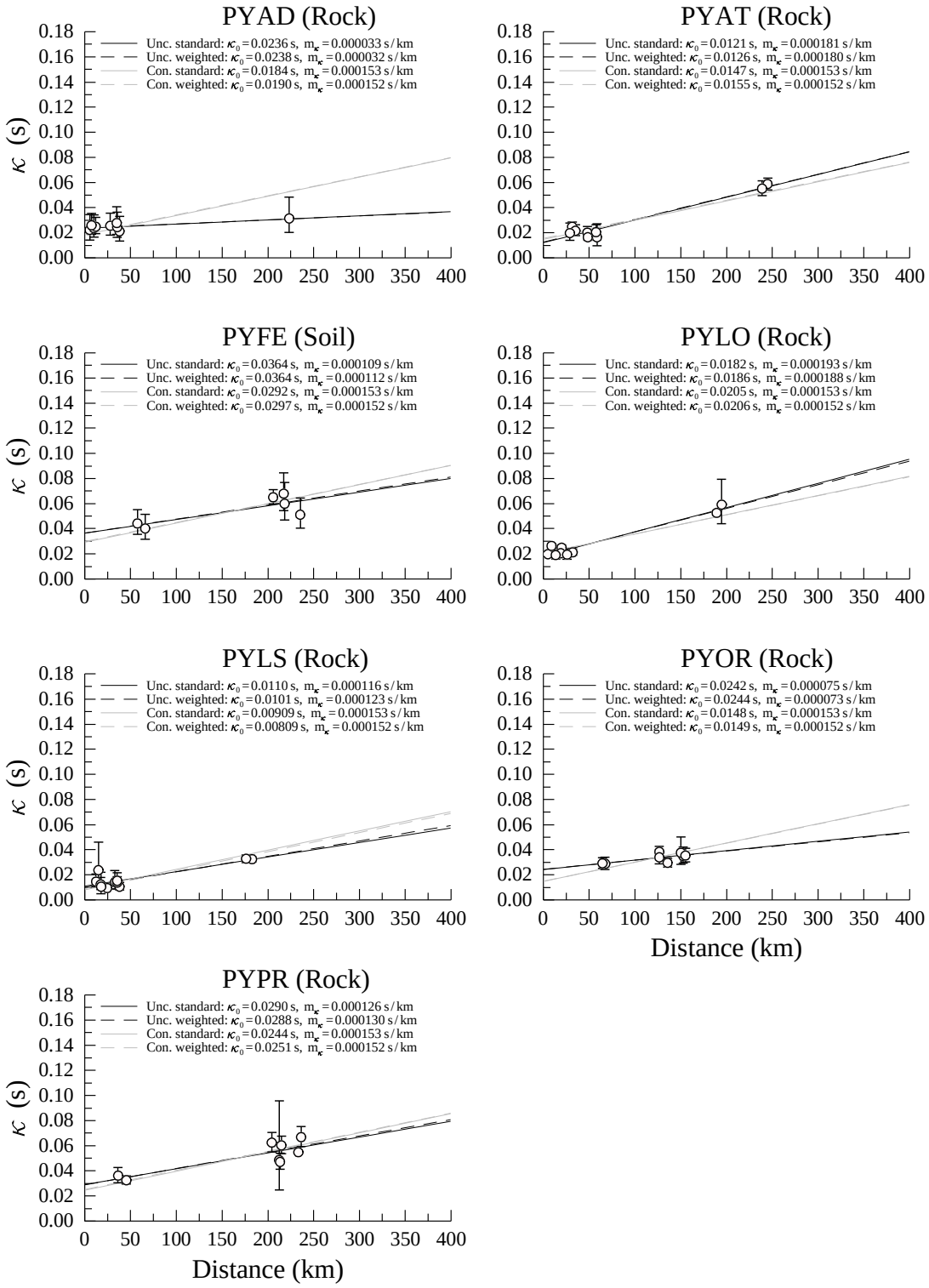


Figure 8: κ estimates and their ± 1 standard deviations for stations located in the Pyrenees. Also shown are the fitted linear relations. Four best-fit lines were fitted for each station: two (using standard and weighted regression) in which m_κ was allowed to vary (black) and two (using standard and weighted regression) in which m_κ was constrained to the value from the regional analysis shown in Figure 6 (grey).

List of Tables

1 Earthquakes and stations used to compute κ. M_w estimates are from Global CMT unless otherwise stated. NS is number of records used from that event. . 25

Table 1: Earthquakes and stations used to compute κ. M_w estimates are from Global CMT unless otherwise stated. NS is number of records used from that event.

YYYY	MM	DD	HH	MM	Lat.(N)	Lon.(E)	M_w	Stations	NS
1996	02	18	04	16	44.74	6.77	3.4 (m_b, ISC)	OGAG	1
1996	07	15	00	13	46.00	6.11	5.3 (CSEM)	OGAG, OGDH, OGSI, SAOF	4
1996	07	23	04	08	45.98	6.01	4.4 (m_b, NEIC)	OGSI	1
1997	02	24	12	06	43.71	8.47	3.7 (m_b, ISC)	CALF, OGDI, SAOF	3
1997	05	15	00	24	45.23	6.62	3.6 (m_b, ISC)	OGMO, OGMU	2
1997	10	03	15	03	44.32	6.45	3.6 (M_L, NEIC)	CALF, OGCA, STET	3
1997	10	31	04	23	44.26	6.57	4.3 (MED RCMT)	CALF, OGAN, OGCU, OGMO, OGMU, OGSI, OGSR, SAOF	8
1997	11	08	01	56	44.07	7.89	3.6 (m_b, ISC)	CALF, OGCA, OGMO, OGMU, SAOF	5
1999	01	11	03	36	45.10	5.76	3.4 (m_b, ISC)	OGAG, OGBL, OGCU, OGDH, OGLE, OGMB, OGMO, OGMU, OGPC, OGSI, STET	11
2000	06	27	04	07	41.25	9.64	4.3 (MED RCMT)	SMPL	1
2001	02	06	22	28	44.12	8.66	4.2 (ZUR RMT)	MENA, NBOR, NLIB, NROC, OGAN, OGCU, OGDI, OGFH, OGLE, OGMO, STET	11
2001	02	25	18	34	43.49	7.47	4.5 (MED RCMT)	ARBF, MENA, NALS, NBOR, NLIB, NPOR, NROC, OGAN, OGBB, OGCH, OGCU, OGDI, OGFB, OGFH, OGLE, OGMO, OGMU, RUSF, SAOF, STET	20
2001	03	03	01	55	41.29	9.76	4.1 (ZUR RMT)	SMPL	1
2001	11	07	09	40	41.73	9.68	4.5 (MED RCMT)	SMPL	1
2002	02	10	16	21	41.23	9.36	3.7 (m_b, ISC)	SMPL	1
2002	05	16	14	56	42.94	-0.16	3.9 (ZUR RMT)	PYAD, PYAT, PYBE, PYFE, PYLO, PYLS, PYLU, PYP1, PYPE, PYPR	10
2002	05	16	15	14	42.82	-0.15	3.8 (m_b, ISC)	PYAD, PYBE, PYFE, PYLO, PYLS, PYP1, PYPR	7
2002	09	05	20	42	43.05	-0.40	4.1 (M_L, LDG)	PYAD, PYLS, PYPR	3
2002	12	11	20	09	43.04	-0.33	3.7 (IAG)	PYAD, PYAT, PYLS, PYOR, PYPP	5
2002	12	12	17	59	43.11	-0.28	4.0 (IAG)	PYAD, PYAT, PYLI, PYLO, PYLS, PYOR, PYPE, PYPM, PYPP	9
2003	01	21	18	00	43.05	-0.36	4.0 (ZUR RMT)	PYAD, PYAS, PYAT, PYFE, PYLO, PYLS, PYOR, PYPP, PYPM, PYPR	10
2003	02	22	20	41	48.31	6.66	5.0	OGAN, OGBL, OGCH, OGEP, OGLE, OGMA, OGMU, OGSR, STBO, STBR, STDM, STFL, STHE, STMU, STSM, STUF	16
2003	02	26	03	32	42.38	2.12	4.4 (M_L, LDG)	PYAD, PYAT, PYBA, PYFE, PYLI, PYLO, PYLS, PYOR, PYPE, PYPM, PYPR, PYPT	12
2004	02	23	17	31	47.30	6.28	4.5 (ZUR RMT)	OGAN, OGAP, OGCH, OGCU, OGEP, OGFB, OGLE, OGMO, OGMU, OGPO, OGSI, OGSR, OGTB, STBO, STBU, STDM, STHE, STSM	18
2004	09	21	15	48	42.34	2.02	4.4 (IAG)	BRGM, PYAS, PYAT, PYBA, PYBE, PYCA, PYFE, PYFO, PYLI, PYLL, PYLO, PYLS, PYOR, PYPE, PYPR, PYPT	16
2005	09	08	11	27	46.01	6.87	4.6	ANTI, BELV, BRGM, CALF, ESCA, ISOL, NREV, OCCD, OGAN, OGAP, OGBB, OGDH, OGCH, OGDI, OGFB, OGFH, OGFM, OGH1, OGH2, OGH3, OGPC, OGPO, OGSI, OGTB, OGTI, SAOF, STET, STFL, STSM	29
2006	09	02	01	21	43.92	7.59	3.6 (m_b, ISC)	ARBF, BELV, CAGN, ESCA, ISOL, MENA, NCAD, NLIB, NROC, NREV, OGCA, OGDI, OGFH, OGGM, OGMO, OGPC, SAOF	17
2006	11	17	18	19	43.08	0.01	4.6 (m_b, ISC)	PYAD, PYAS, PYAT, PYBB, PYBE, PYFE, PYFO, PYLI, PYLO, PYLS, PYLU, PYOR, PYPC, PYPM, PYPP, PYPR, PYPU, PYTB	18
2006	12	16	08	17	42.99	-0.13	4.1 (M_L, LDG)	PYAT, PYBB, PYLO, PYLS, PYOR, PYPC, PYPR, PYPU, PYTB	9
2007	11	15	13	47	43.02	-0.01	4.5 (M_L, LDG)	PYAD, PYAS, PYAT, PYBB, PYBE, PYLO, PYLS, PYOR, PYPC, PYPU, PYTB	11
			30 events				3.4 (m_b)–5.3 (M_w)	83 different stations	263